Electronic Supporting Information (ESI) for

Spark plasma sintered catalytic nickel-copper alloy and carbon nanotube electrodes for hydrogen evolution reaction

Jean-Felix Boue,[ab] Cedric Espinet,[a] Simon Amigues,[a] David Mesguich,[b] David Cornu,[bc] Yaovi Holade,*[ac] Julien Cambedouzou,*[ac] and Christophe Laurent*[b]

[a] *Institut Européen des Membranes, IEM, UMR 5635, Univ Montpellier, ENSCM, CNRS, 34090 Montpellier, France.*

[b] *CIRIMAT, Université Toulouse 3 Paul Sabatier, CNRS, Université de Toulouse, 118 Route de Narbonne, 31062 Toulouse cedex 9, France*

[c] *French Research Network on Hydrogen (FRH2), Research Federation No. 2044 CNRS, BP 32229, 44322 Nantes CEDEX 3, France, https://frh2.cnrs.fr/.*

Corresponding authors : E-mail: yaovi.holade@enscm.fr (Y.H.), julien.cambedouzou@enscm.fr (J.C.), christophe.laurent@univ-tlse3.fr (Ch.L.).

Table of Contents

EXPERIMENTAL METHODS

Materials and chemicals.

Nickel (II) nitrate hexahydrate [$Ni(NO_3)_2{\cdot}6H_2O$, 99%, Thermo Scientific], copper (II) trihydrate [$Cu(NO_3)_2{\cdot}3H_2O$, 99.5%, Merck], urea [$CO(NH_2)_2$, >99%, Sigma Aldrich], potassium permanganate ($KMnO_4$, ≥99%, Sigma-Aldrich), hydrogen peroxide solution (H_2O_2, 30%, Sigma-Aldrich), sulfuric acid (H_2SO_4, 97%, Honeywell), sodium hydroxide [NaOH, 99%, BAKER, J.T.Baker™], multi-walled carbon nanotubes [CNT, Nanocyl, Belgium (BET specific surface area = 242 $m^2\ g^{-1}$, average number of CNT walls = 8, average CNT external diameter = 10 nm, maximum CNT length = 1.5 µm)[1]], and commercial catalyst Pt/C (20 wt%, 2 nm, Premetek Co., USA) were used as-received. N_2 (grade 4.5) gas was purchased from Air Liquide (France) and used as-received. Ultrapure water (18.2 MΩ cm at 20 °C) was produced by a Milli-Q Millipore source (MQ).

Synthesis of Ni-Cu oxides powder (hereafter referred to as "raw powder"). A powder made up of an intimate mixture of NiO and CuO was prepared by the nitrate-urea combustion route.[2] In a typical synthesis of 12 g of sample, 35.468 g of $Ni(NO_3)_2{\cdot}6H_2O$ and 9.548 g of $Cu(NO_3)_2{\cdot}3H_2O$ (corresponding to the targeted Ni:Cu atomic proportion of 3:1) and 79.260 of $CO(NH_2)_2$ were dissolved in an Inconel dish with 50 mL of ultrapure water at 60 °C under a moderate magnetic stirring. After completed dissolution, the dish was placed in a furnace preheated at 700 °C, keeping the door open for the entire process. After water evaporation, the combustion reaction took place. As detailed elsewhere,[3,4] it is difficult to establish the proportion of fuel (urea) to be used for such a redox reaction. When using the so-called stoichiometric proportion calculated using the total oxidizing valence of the nitrates and reducing valence of urea, the combustion is very violent, resulting in copious projections out of the dish. We gradually increased the proportion of urea and after optimization this led to a mild combustion (duration of about 10 min). The proportion of urea was fixed at 5 times the so-called stoichiometric proportion and therefore we note that the reaction was performed in reducing (fuel-rich) conditions.

Mixing with CNTs : ball-milling, sonication and lyophilization. The so-obtained powder was ball-milled in order to break the agglomerates (PM 100 Retsch planetary mill, tetragonal-zirconia balls and vessel, 1 h, 400 rpm, rotational direction change every 5 min with a 30 s break). Then, a suspension of the suitable quantity of ball-milled powder (different quantity in 40 mL of ultrapure water, sonicated for 15 min) was poured into a CNT suspension (110 mL of ultrapure water, sonicated for 15 min) and the mixture was sonicated for 15 min before lyophilization (Christ alpha 2–4 LD, Bioblock Scientific, -40 °C, 12 Pa, 96 h). Five oxide-CNT powders with different oxide proportions were prepared: 1.2, 2.4, 6, 15 and 25 wt%.

Consolidation by spark plasma sintering (SPS). A schematic diagram of SPS is shown in Figure S1. The sample is loaded into a graphite die, which is placed between graphite punches. The graphite/punches ensemble is known as the stack. SPS involves the passing of a high-intensity pulsed direct electrical current through the sample and/or stack, depending on their respective electrical conductivity, whereas a uniaxial load is applied on the sample. This allows consolidating powders compacts, fully or not, into simple or complex shapes, at lower temperatures and for much lower durations (typically 30 min) than other sintering techniques.

More details can be found in a recent review of the field[5]. The oxide-CNT powders were consolidated by Spark Plasma Sintering (SPS, Dr Sinter 2080, SPS Syntex Inc., Japan) using experimental conditions that were found to be appropriate for 8-walled CNT monoliths[6]. Typically, 150 mg of the above material were loaded into an 8 mm inner diameter graphite die. For the sake of easy removal, a spray of graphite was applied on the punch and a sheet of graphitic paper was placed between the die and the powder. The SPS run was performed in vacuum (residual cell pressure < 12 Pa) using the default pattern of the machine (12 on:2 off) 3.3 ms current pulses. A heating rate of 300 °C min^{-1} was used from room temperature to 600 °C, where a 1 min dwell was applied. A uniaxial charge was gradually applied during the ramp and dwell to reach a value of 100 MPa on the pellet. Then, a heating rate of 100 °C min^{-1} was applied to reach a maximum temperature of 1300 °C, where a 3 min dwell was applied. The temperature is controlled by an optical pyrometer focused on a little hole at the outer surface of the die. Natural cooling was applied down to room temperature and the uniaxial load was gradually released during the same time. Note that the experimental conditions in the SPS cell are reducing. The samples obtained were in the form of pellets 8 mm in diameter and 1.0 to 1.5 mm thick. They are designated E_m hereafter, with E for electrode and *m* corresponding to the metal content in wt%. Five (5) pellets were prepared, referred to as E1, E2, E5, E12 and E20. Note that the oxides (NiO and CuO) are reduced during SPS, forming a metal alloy, with a possible composition distribution.

Physicochemical characterization. X-ray diffraction (XRD, Cu Kα radiation, Bruker D4 Endeavor) was used to detect and identify crystalline phases. The powders were observed by field-emission-gun scanning electron microscopy (FESEM, JEOL JSM 6700F). The density of the electrodes was calculated from their weight and geometric dimensions. Scanning electron microscopy (SEM) observation of the pellets was performed on a Hitachi S-4800 microscope. N_2 adsorption-desorption isotherms of pellet samples were measured at liquid N_2 temperature (Micromeritics ASAP 2020). The samples were degassed by heating at 120 °C under a primary vacuum for 12 h. The Brunauer-Emmett-Teller (BET) specific surface area (S_{BET} in $m^2\ g^{-1}$) was determined in the relative pressure (P/P°) range 0.05 - 0.3. The Barrett-Joyner-Halenda (BJH) method applied on the desorption branch of the isotherm was used to determine the specific pore volume (at P/P° = 0.99) and the pore size distribution (PSD).

Electrochemical measurements. The used potentiostat was VIONIC (Metrohm). The glassware used in electrochemistry was immersed for a minimum of 12 hours in an acidified potassium permanganate solution to remove all impurities [$KMnO_4$ at 3 g L^{-1} and H_2SO_4 at 2.25 mol L^{-1}]. The glassware was washed with a solution made of 1/3 water, 1/3 H_2SO_4 and 1/3 H_2O_2. We use cold and hot water to rinse everything in the following order: cold, hot, cold. The hydrogen evolution reaction (HER) efficiency of the electrodes was evaluated in a conventional three-electrode set-up at 25 °C by methods of linear sweep voltammetry (LSV) and chronopotentiometry (-100 mA cm^{-2}). The working electrode was the pellet prepared by SPS (cylinder 8 mm in diameter and 1.25 ± 0.25 mm thick), which leads to a geometric external surface area of 1.3-1.4 cm^2, which was used for normalization of the current density. Electrical connection was ensured by a gold wire (minor contribution to HER in the potential range of interest, -0.4 to 0 V *vs* RHE). The counter electrode was a glassy carbon plate and the reference electrode was a mercury-mercury oxide electrode (MOE) Hg|HgO|1 M NaOH. The electrolyte (1 M NaOH) was purged for 30 min with argon before any measurement. The working electrode was conditioned electrochemically by cyclic voltammetry (CV, fifty cycles, 100 mV s^{-1}) before running six LSV (5 mV s^{-1}) to obtain quasi-stable LSV curves. LSV curves were ohmic-drop-corrected (the ohmic resistance was 0.9-1.3 Ω in all measurements), and the potentials were converted versus reversible hydrogen electrode based: E(V vs RHE) = E(V vs MOE) + ΔE, with ΔE = 1.01 V obtained from a calibration curve in H_2-saturated 1 M NaOH solution at 25 °C. For the commercial catalyst Pt/C (20 wt%, 2 nm, Premetek Co., USA) prepared for the sake of comparison, the catalytic ink was prepared by mixing 130 µL of ultrapure water, 50 µL of ethanol, 20 µL of Nafion (5 wt%) and 5 mg of catalyst powder. The mixture was ultra-sonicated for at least 30 min. The homogenous ink that was drop-casted onto each face of a L-shaped carbon paper (AvCarb MGL190, 190 µm thickness, Fuel Cell Store) electrode of 0.5 cm^2 and the solvent was evaporated under room temperature to reach ca. 0.1 mg cm^{-2}.

DISCUSSION AROUND WATER ELECTROLYSIS

Liquid alkaline water electrolysis (AWE) has been used for industrial hydrogen production since the 1900s[7] and is therefore the most mature hydrogen production technology using electrochemical water splitting. The main advantage of this technology is the use of non-noble

metals catalysts. The solid polymer electrolyte (SPE) based proton exchange membrane water electrolysis (PEMWE) is the other hydrogen production technology which is most advanced and with the higher performance.[8] The main drawback being the use of noble metals as catalysts (to insure the chemical stability) leading to price volatility and geopolitical issues. Other technologies such as hydroxide anion exchange membrane water electrolyzer (AEMWE), solid oxide electrolysis cell (SOEC) or proton conducting ceramic electrolyzer (PCCEL) are known[8] but their industrial utilization needs further optimization.

A recent Open Access Review-article (2022)[8] provides an extended analysis of the different systems and the full history (from seminal literature references to Key performance indicators (KPI) and technology targets). AEMWE and PEMWE,[8,9] are considered the most promising technologies for overcoming some of the drawbacks of AWE: increased ohmic drop (caused by H_2 and O_2 bubbles in the liquid electrolyte, altering ionic conductivity), possible mixing between H_2 and O_2 bubbles (because the separator is porous) leading to safety and gas purity problems, and the operation conditions (temperature, duration, etc.) needed to reach a steady-stage functioning.[8] These points are not common with dense separators based on SPE technology such as AEMWE and PEMWE. For the latter, the reduction of the strategic metals content is need to supply the rapid growth of the H_2 demand. At the cathode, for platinum, it is currently around 1-5 mg cm^{-2},[8,9] and even a reduction to 0.1 mg cm^{-2} to drastically reduce the electrode cost will lead to large total amount of Pt per electrolyzer. An alternative is to develop efficient non-noble metal catalysts for AEMWE for which a significantly reduced amount of strategic and/or non-noble metals will be required in certain parts of the world. We think that reducing the noble metal catalyst loading represents a short-term solution since the price volatility and geopolitical issues will still exists even with low loadings, indeed hydrogen production facilities number will increase in the coming years on a worldwide scale so the demand for noble metals will increase. Developing efficient non-noble metal catalyst for AEMWE or engineering tridimensional carbon-based electrodes with a small amount of catalytic metals in AWE (reduce the overall cost of the devices compared to nickel coated perforated stainless steel), will allow for more independence on few resources for some countries.

Table S1. Specific surface area and porosity data of the electrode prepared by SPS from N_2 adsorption–desorption isotherms.

Electrode	BET specific surface area ($m^2\ g^{-1}$)[a]	Average pore size (nm)[b]	Specific pore volume ($cm^3\ g^{-1}$)[c]
E1	190	4.4	0.234
E2	199	4.3	0.232
E5	203	5.0	0.265
E12	155	4.9	0.217
E20	121	4.9	0.178

[a] Calculated by the Brunauer-Emmett-Teller (BET) method, using the adsorption branch of the N_2 isotherm for the relative pressure P/P° = 0.05-0.3.

[b] Calculated by the Barrett-Joyner-Halenda (BJH) method, using the desorption branch of the N_2 isotherm.

[c] BJH desorption cumulative volume of pores (width between 1.7 and 300 nm).

Table S2. Comparative HER performance of relevant nickel-based electrocatalysts in alkaline media. η_j (mV) is a notation for the overpotential at the current density j(mA cm^{-2}).

Ref.	Electrocatalyst [metal content, wt%]		Electrode material		HER	
			Free-standing ?	electrode preparation	Electrolyte [temperature]	Performance
This work	Mesoporous electrocatalytic electrodes based on nickel-copper nanoalloys and carbon nanotube consolidated by spark plasma sintering (SPS) for different metal content [wt%]	1	Yes	Working electrode = cylinder of 8 mm diameter and 1.0-1.5 mm thickness, which lead to geometric area of 1.3-1.4 cm^2	1 M NaOH [25 °C]	η_{10} = 240 mV η_{50} >350 mV
		2				η_{10} = 210 mV η_{50} >350 mV
		5				η_{10} = 170 mV η_{50} >350 mV
		12				η_{10} = 167 mV η_{50} = 310 mV
		20				η_{10} = 161 mV η_{50} = 327 mV
		Most performant electrode (5 wt%)				η_{10} = 161 mV η_{50} = 279 mV Stability: chronopotentiometry at -100 mA cm^{-2} for 24 h [post-mortem η_{10} = 132 mV at -10 mA cm^{-2} and η_{50} = 235 mV]
10	NiCu alloy		No	Catalytic ink (catalyst NiCu + isopropanol + Nafion ionomer + water) drop-cast onto 5 mm GCE	1 M KOH [20 °C]	η_{10} = 200 mV η_{50} = 355 mV

11	Nitrogen-doped graphene-encapsulated nickel–copper alloy (Ni_3Cu_1@NG-NC)	No	Catalytic ink (catalyst + ethanol + water + Nafion ionomer) drop-cast onto 5 mm GCE	1.0 M KOH [unknown temperature]	η_{10} = 122 mV η_{50} = 250 mV Stability: chronopotentiometry at -40 mA cm^{-2} for 40 h, overpotential = 240 mV
12	Freestanding Surface Disordered NiCu	Yes	$Ni_{0.95}Cu_{0.05}$ freestanding porous metallic film prepared in an autoclave at 160 °C for 2 h (0.25 cm^2)	1 M KOH [25 °C]	η_{10} = 70 mV η_{50} =130 mV Stability: chronopotentiometry at -1000 mA cm^{-2} for 110 h
13	3D porous hierarchical Ni–Fe phosphate film/Ni foam	Yes	Electrodeposition of NiFe-P by cyclic voltammetry on a Ni foam scaffold	1 M KOH [25 °C]	η_{10} = 87 mV η_{50} =170 mV Stability: chronopotentiometry at -10 mA cm^{-2} for 12 hours [post-mortem η_{10} = 95 mV]
14	Ni nanoparticles supported on graphene layers [68.9 wt%]	Yes	Ni-rGO (reduced graphene oxide) catalyst prepared by supergravity electrodeposition on nickel foam (10x10 mm)	1 M KOH [25 °C]	η_{10} = 36 mV η_{50} = 120 mV Stability: chronopotentiometry at -250 mA cm^{-2} for 10 h, at -100 mA cm^{-2} for 20 h, at -250 mA cm^{-2} for 10 h
15	NiS microsphere synthetized on Ni foam	Yes	NiS microsphere synthetized on Ni foam	1 M KOH [unknown temperature]	η_{10} = 130 mV η_{50} = 190 mV Stability: cyclic voltammetry at 100 mV s^{-1} for 1000 cycles [post-mortem η_{50} =190 mV]
16	NiCu synthesized onto copper substrate	Yes	NiCu catalyst galvanostatically deposited on a copper substrate	1 M KOH [22 °C]	η_{10} = 229 mV
17	Nanoscale nickel oxide/nickel heterostructures	No	$Ni(OH)_2$/ox-CNT dispersed in ethanol and drop dried on Ni foam: [8 mg cm^{-2}]	1 M KOH [23 °C]	η_{10} = 40 mV η_{50} =70 mV Stability: chronopotentiometry at -20 mA cm^{-2} for 2 hours [post-mortem η_{20} = 45 mV]

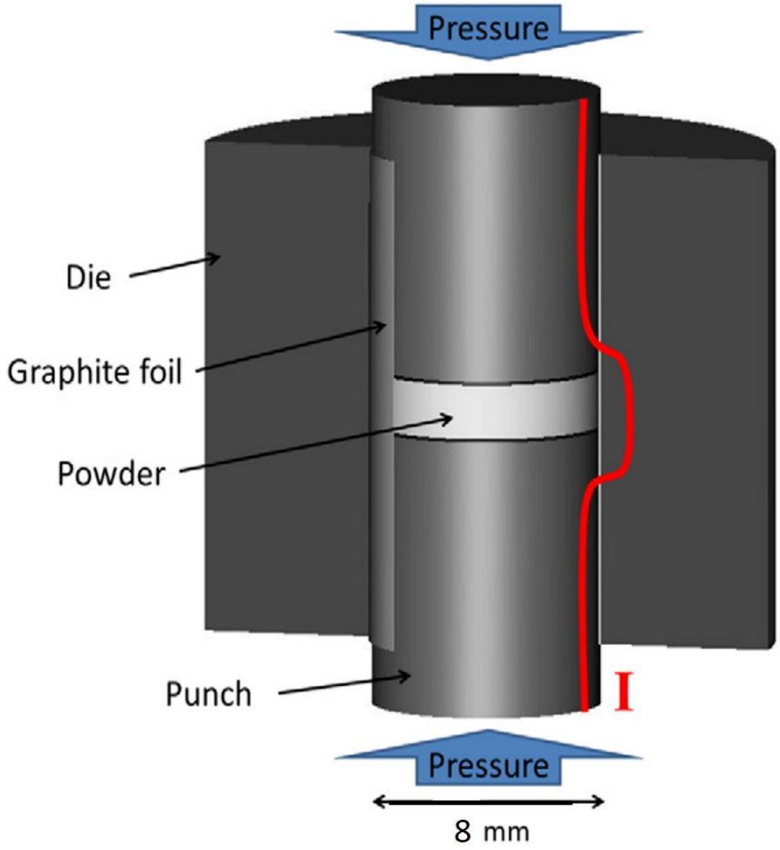

Fig. S1. Schematic diagram of the SPS method.

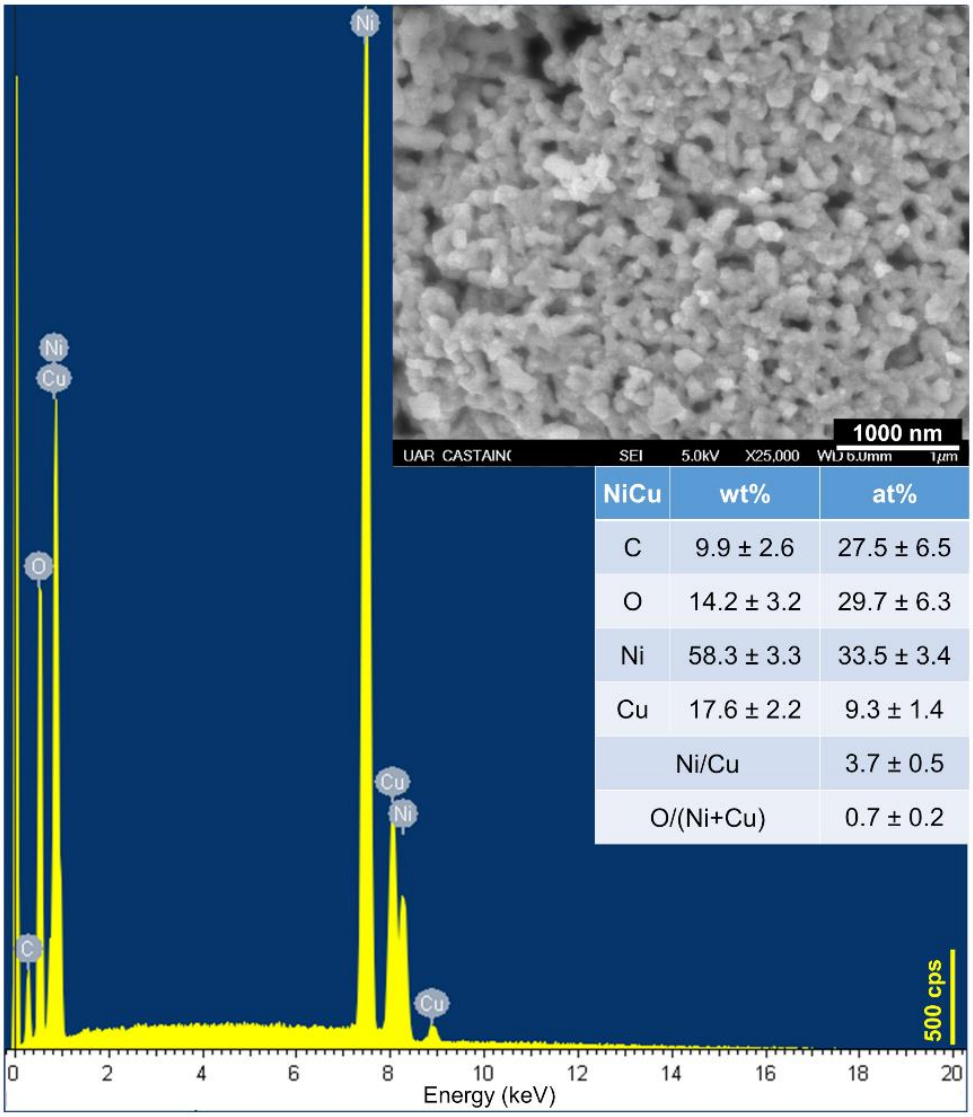

NiCu	wt%	at%
C	9.9 ± 2.6	27.5 ± 6.5
O	14.2 ± 3.2	29.7 ± 6.3
Ni	58.3 ± 3.3	33.5 ± 3.4
Cu	17.6 ± 2.2	9.3 ± 1.4
Ni/Cu		3.7 ± 0.5
O/(Ni+Cu)		0.7 ± 0.2

Fig. S2. EDX spectra, backscattered SEM image and quantitative analysis on the synthesized Ni-Cu.

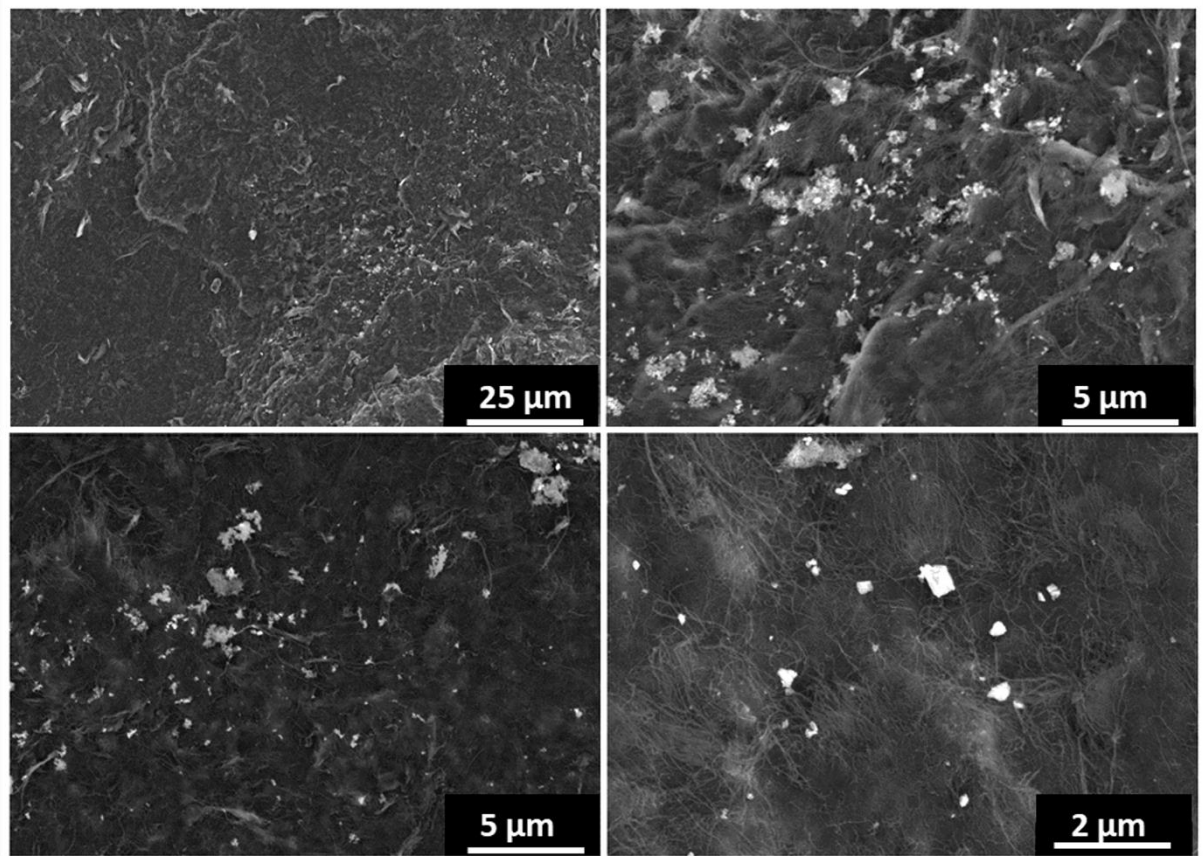

Fig. S3. SEM images (backscattered electron mode) of the E5 electrode prepared by SPS showing the Ni-Cu nanoparticles (appearing white on the images) and the CNTs.

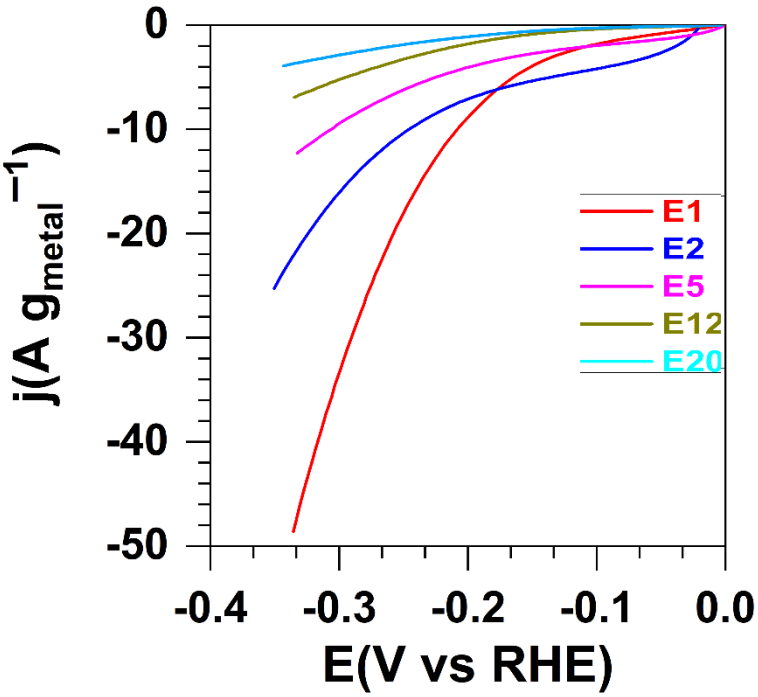

Fig. S4. HER performance of the electrodes (1 M NaOH, 25 °C) prepared by SPS: Ohmic-drop LSV (5 mV s^{-1}) corrected by the metal content.

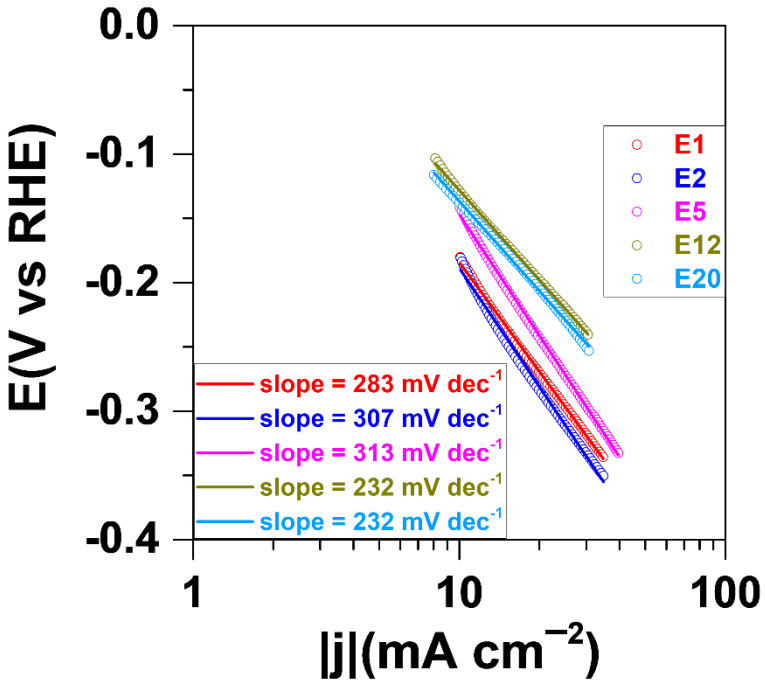

Fig. S5. HER performance of the electrodes (1 M NaOH, 25 °C) prepared by SPS: Tafel plots from ohmic-drop corrected LSV (5 mV s^{-1}).

Supplementary References.

1. Ch. Guiderdoni, E. Pavlenko, V. Turq, A. Weibel, P. Puech, C. Estournès, A. Peigney, W. Bacsa and Ch. Laurent, Carbon, 2013, **58,** 185-197.
2. K. C. Patil, *Bull. Mater. Sci.*, 1993, **16**, 533-541.
3. Y. Zhang and G. C. Stangle, *J. Mater. Res.*, 2011, **9**, 1997-2004.
4. P. Coquay, E. De Grave, A. Peigney, R. E. Vandenberghe and C. Laurent, *J. Phys. Chem. B*, 2002, **106**, 13186-13198.
5. Z.Y. Hu, Z.H. Zhang, X.W. Cheng, F.C. Wang, Y.F. Zhang and S.L. Li, Materials and Design 191 (2020) 108662
6. C. Laurent, T. M. Dinh, M. C. Barthélémy, G. Chevallier and A. Weibel, *J Mater Sci*, 2018, **53**, 3225-3238.
7. C.T. Bowen, H.J. Davis, B.F. Henshaw, R. Lachance, R.L. LeRoy, R. Renaud, *International Journal of Hydrogen Energy* , 1984, **9**, 59-66
8. M. Chatenet, B. G. Pollet, D. R. Dekel, F. Dionigi, J. Deseure, P. Millet, R. D. Braatz, M. Z. Bazant, M. Eikerling, I. Staffell, P. Balcombe, Y. Shao-Horn, H. Schäfer, *Chem. Soc. Rev.*, 2022, **51**, 4583-4762
9. IRENA**,** Green Hydrogen Cost Reduction: Scaling up Electrolysers, 2021
10. A. Y. Faid, A. O. Barnett, F. Seland and S. Sunde, *Electrochim. Acta*, 2021, **371**, 137837.
11. B. Liu, H.-Q. Peng, J. Cheng, K. Zhang, D. Chen, D. Shen, S. Wu, T. Jiao, X. Kong, Q. Gao, S. Bu, C.-S. Lee and W. Zhang, *Small*, 2019, **15**, 1901545.
12. X. Zhang, J. Wang, J. Wang, J. Wang, C. Wang and C. Lu, *J. Phys. Chem. Lett.*, 2021, **12**, 11135-11142.
13. J. Xing, H. Li, M. Ming-Cheng Cheng, S. M. Geyer and K. Y. S. Ng, *J. Mater. Chem. A*, 2016, **4**, 13866-13873.
14. L. Wang, Y. Li, M. Xia, Z. Li, Z. Chen, Z. Ma, X. Qin and G. Shao, *J. Power Sources*, 2017, **347**, 220-228.
15. W. Zhu, X. Yue, W. Zhang, S. Yu, Y. Zhang, J. Wang and J. Wang, *Chem. Commun.*, 2016, **52**, 1486-1489.
16. X.-D. He, F. Xu, F. Li, L. Liu, Y. Wang, N. Deng, Y.-W. Zhu and J.-B. He, *J. Electroanal. Chem.*, 2017, **799**, 235-241.
17. M. Gong, W. Zhou, M.-C. Tsai, J. Zhou, M. Guan, M.-C. Lin, B. Zhang, Y. Hu, D.-Y. Wang, J. Yang, S. J. Pennycook, B.-J. Hwang and H. Dai, *Nat. Commun.*, 2014, **5**, 4695.